Scanning Approaches of 2-D Resistive Sensor Arrays: A Review

Jian-Feng Wu

***Abstract*— With scanning approaches of low complexity, the 2-D resistive sensor arrays (RSAs) are used to extract the distribution of sensed variable values (e.g., physical pressure) over the sensing area. This review surveys the scanning approaches of the 2-D RSAs, their evaluation methods, and their applications. The principle of the 2-D RSA with the scanning approach is introduced first. Then, different scanning approaches of RSAs are illustrated. The scanning approaches of RSAs are mainly categorized into the inserting diode method, the inserting transistor method, the passive integrator method, the resistance matrix approach, the incidence matrix approach, the voltage feedback method, the zero potential method, and so on. Next, various evaluation methods of the scanning approaches are presented. The scanning approach's evaluation methods are categorized into testing of the actual system, analyzing with circuit simulation software, and analyzing with test model. Followed, typical applications of the 2-D RSAs with the scanning approaches and their special requirements are analyzed. Finally, the characteristics of various typical scanning approaches and their development tendency are discussed and investigated in detail.**

***Index Terms*— 2-D resistive sensor array, scanning approach, measurement error, readout circuit, circuit model.**

ABBREVIATION INDEX

2-D	Two-dimensional
RSA	Resistive sensor array
IDM	Inserting diode method
ITM	Inserting transistor method
PIM	Passive integrator method
RMA	Resistance matrix approach
IMA	Incidence matrix approach
VFM	Voltage feedback method
ZPM	Zero potential method
3-D	Three-dimensional
EBT	Element being tested
PSR	Pressure sensitive resistor
FPGA	Field Programmable Gate Array
ADC	Analog-to-digital converter
CS	Current source
EIT	Electrical Impedance Tomography
VF-NSE	Voltage feedback non-scanned-electrode
VF-NSSE	Voltage feedback non-scanned-sampling-electrode
VF-NSDE	Voltage feedback non-scanned-driving-electrode
IDFC	Isolated Drive Feedback Circuit
IIDFC	Improved Isolated Drive Feedback Circuit
IIDFCC	Improved Isolated Drive Feedback Circuit with Compensation
PVG	Part virtual ground
FVG	Full virtual ground
S-NSE-ZP	Setting non-scanned-electrode zero potential
S-NSSE-ZP	Setting non-scanned-sampling-electrode zero potential
S-NSDE-ZP	Setting non-scanned-driving-electrode zero potential
S-NSE-EP	Setting non-scanned-electrode-equipotential
S-NSSE-EP	Setting non-scanned-sampling-electrode-equipotential
S-NSDE-EP	Setting non-scanned-driving-electrode-equipotential
VFC	Voltage feedback circuit
ZPC	Zero potential circuit
RRAM	Resistive random-access memory
RC	Resistance-capacitance

Manuscript received September 15, 2016; revised November 23, 2016; accepted December 13, 2016. Date of publication December 19, 2016; date of current version January 19, 2017. This work was supported in part by the Specialized Research Fund for the Doctoral Program of Higher Education under Grant 20130092110060, in part by the National Major Scientific Equipment R&D Project under Grant ZDYZ2010-2, in part by the Natural Science Foundation of China under Grant 61571113, Grant 61304205, and Grant 61502240, and in part by the Natural Science Foundation of Jiangsu Province under BK20141002. The associate editor coordinating the review of this paper and approving it for publication was Prof. Pantelis Georgiou.

The author is with the Jiangsu Key Laboratory of Remote Measurement and Control, School of Instrument Science and Engineering, Southeast University, Nanjing 210096, China (e-mail: wjf@seu.edu.cn).

Digital Object Identifier 10.1109/JSEN.2016.2641001

I. INTRODUCTION

WITH every sensitive element as a discrete resistor, the 2-D RSAs are used to perceive the physical parameters distributed in the sensing area. In the traditional resistance measurement approach, a large number of connected wires and measuring circuits, for example $M \times N + 1$ [1], are necessary for accessing all elements in the $M \times N$ RSA. By taking electrical excitation signals and potential measurements only at the shared wires, some scanning approaches of the 2-D RSAs with shared row-column wires have been proposed for reducing the connection wire number. Two sets of interconnection wires are used in these scanning approaches with all the sensor elements having one end connected to a row wire and the other end connected to a column wire. So $M + N$ interconnect wires are used in the $M \times N$ RSA. But the crosstalk effect caused by parasitic parallel paths of shared wires influences the performance of these scanning approaches in RSAs. With less crosstalk effect, the application of the IDM [2]–[4] in the 2-D RSA was firstly described by Snyder *et al.* [2] in 1978, and then different kinds of scanning approaches of the 2-D RSAs emerged rapidly, such as the ITM [5]–[8], the PIM [9]–[11],

the RMA [12], the IMA [13], the VFM [14]–[23], the ZPM [24]–[30], *etc*. Compared to traditional measurement method, scanning approaches of RSAs have many advantages such as few wires, low complexity, low cost, high precision, easy integration, *etc*. As a result, the scanning approach of the 2-D RSA is widely applied in many fields including tactile sensor [2], [3], [8], [9], [12], [14], [15], [31], [33], artificial electronic skin [34]–[38], chemical sensor [39], [40], man-machine interaction input device [41], [42], and imaging sensor [5], [43]–[47].

RSAs based on scanning approaches have the potential to provide a low cost, easy-to-manufacture solution to the problem of the flexible, stretchable large-scale sensing applications, for example artificial electronic skin. However, the RSA's properties including flexibility, stretchability, and array size, affected its performances such as sensing range, sensitivity, readout rate, power consumption, and their robust to noise. At the same time, principles, structures, and processes of the RSA with the scanning approaches have been changing rapidly in recent years. In this review, we will mainly focus on the recent RSA's readout circuitry technologies, their evaluation methods, and their applications. Following this introductory section, Section 2 introduces the principles and the performance metrics of the scanning approaches. Section 3 presents the evaluation methods of the scanning approaches. A general overview of applications of the 2-D RSAs with the scanning approaches is presented in Section 4, which is followed by discussion and conclusion in Section 5.

II. Scanning Approaches of RSAs

Various scanning approaches with low complexity of interconnection were proposed for eliminating the bypass crosstalk which affected the performances of the 2-D RSAs.

A. The Inserting Diode Method

With the IDM, Snyder *et al.* [2] firstly used diodes to obtain unidirectional currents of all sensitive elements on the same column. As shown in Fig.1 [3], parasitic parallel currents on the non-scanned elements were eliminated and a 40 × 24 RSA with a scanning rate of 300 Hz was used in dynamic contact stress analysis. Ding [4] made an attempt to eliminate the bypass crosstalk of a 3-D RSA with the IDM.

In Fig.1, every sensitive element was connected in series with a diode, shared row wires and shared column wires were used as sampling electrodes and driving electrodes respectively. Parasitic parallel currents on the non-scanned elements were blocked by the unidirectional conductivity of the inserting diodes. For every element being tested (EBT), its row adjacent elements were isolated from its test current path. Through the insert diodes on the scanning column, currents from the excitation voltage source flowed to the scanning elements on a single column of the sensor matrix and then flowed through the sampling resistors to the ground. Therefore, in the IDM, the EBT's output voltage (V_{outIDM}) could be calculated with (1). Also a high readout rate could be achieved for all elements on the same column could be tested simultaneously.

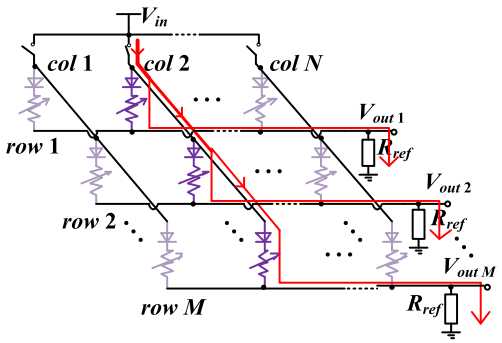

Fig. 1. Schematic of an $M \times N$ sensor array with the IDM (R_{ref}s are the resistances of the reference resistors, V_{in} is the excitation voltage, and V_{outi}s are the EBT's output voltages on the selected column) [3].

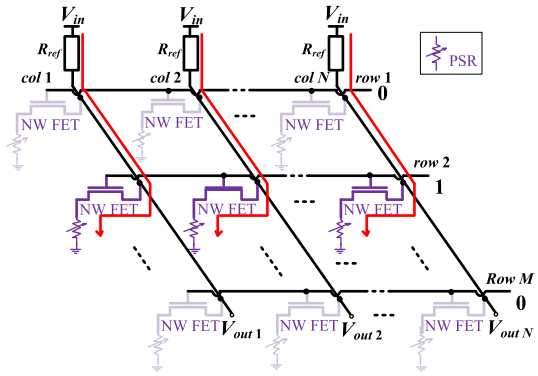

Fig. 2. Schematic of an $M \times N$ sensor array with the ITM (R_{ref}s are the reference resistances, V_{in} is the excitation voltage, and V_{outi}s are the EBT's output voltages on the selected row) [6].

$$V_{outIDM} = \frac{(V_{in} - V_{diode}) \times R_{ref}}{R_{EBT} + R_{ref}} \tag{1}$$

where, the V_{diode} is the drop voltage on the inserting diode, and the R_{EBT} is the EBT's resistance.

But measurement accuracy in the IDM is affected by the V_{diode} which is susceptible to be affected by variations of test current and temperature. Complicated structure of one diode for every sensitive element in the IDM also limits its application.

B. The Inserting Transistor Method

With the ITM, Tanaka *et al.* [5] firstly used transistors to choose the sensitive elements on the same row and realized a 128 × 128 resistive bolometer array with a scanning rate of 30 Hz. In Fig.2 [6], the ITM was also used in an 18 × 19 flexible PSR array with its scanning rate of 5 Hz [6] and a user-interactive electronic skin for instantaneous pressure visualization [7]. With the ITM, Kane *et al.* [8] reported a 64 × 64 resistive stress sensor array with a high-resolution robotic tactile imaging within a 19.2 mm × 19.2 mm sensing area.

As shown in Fig.2 [6], every PSR in the ITM-based RSA was connected in series with a transistor, shared row wires and shared column wires were used as row selection wires

and sampling electrodes respectively. For isolating the adjacent elements on the non-scanned rows from the EBT's test current path, parasitic parallel currents on the EBT's non-scanned elements were blocked by turning off their insert transistors. Through the reference resistors (R_{ref}s), currents from the excitation voltage source flowed to the insert transistors on a single row of the sensor matrix and then flowed through the scanning elements to the ground. With row selection wires and the inserting transistors, the elements on the same row were selected and tested synchronously and a high scanning rate was achieved. In the ITM, the output voltage (V_{outITM}) of the EBT could be calculated with (2).

$$V_{outITM} = \frac{(V_{in} - V_{transistor}) \times R_{EBT}}{R_{ref} + R_{EBT}} + V_{transistor} \quad (2)$$

where, the $V_{transistor}$ is the transistor's drain-source voltage.

But measurement accuracy of the ITM is affected by the transistor's discrete drain-source voltage. Complicated structure of one transistor for every sensitive element in the ITM also limits its application in RSAs.

C. The Passive Integrator Method

The application of the PIM in the 2-D RSA as shown in Fig.3 [9] was firstly described by Fernando *et al.*, who used op-amps with capacitive feedback and FPGA to carry out the sensor-digital conversion of the sensitive elements on the same row and realized a 16 × 16 resistive force sensor array with its scanning rate of 182 Hz and its measurement accuracy of 0.67%. Accuracy analysis [10], resolution analysis [10], and improvement [11] were also implemented on the PIM.

In the PIM, by measuring a discharge time through a capacitor (C_j, $j = 1$ to N) at each column of the matrix, the $M \times N$ RSA was directly connected to the FPGA without the need of independent ADCs to obtain resistance values. The PIM for low-medium size arrays with a simple circuit structure was shown in Fig.3(a) [9], in which calibration resistors (R_{cj}s, $j = 1$ to N) were used to reduce measurement error caused by the drifting of the values of C_js, V_{DD} and V_{TL} for variations of time, power voltage, and temperature. In it, by measuring the discharging times on the C_j for the EBT and the calibration resistor respectively, the EBT's resistance (R_{ij}, $i = 1$ to M, $j = 1$ to N) could be calculated with (3). In series with the R_{ij}, the impedance associated to the pins in the FPGA was added to the result of the measurement in the PIM for low-medium size arrays, which was not feasible for large-scale arrays for its requirement of $(M + 2) \times N$ pins in the $M \times N$ RSA, for example 288 pins in the 16 × 16 array [9].

$$R_{ij} = (t_{Dj}/t_{Dcj})R_{cj} \quad (3)$$

where, t_{Dj} and t_{Dcj} are the discharging times for the R_{ij} and the R_{cj} respectively.

In the PIM for large arrays as shown in Fig.3(b) [9], by measuring a discharge time on an op-amp with capacitive feedback of a capacitor (C_j, $j = 1$ to N) in each column of the matrix, the $M \times N$ RSA was directly connected to the FPGA without the need of independent ADCs to obtain resistance values. Directly connected to the I/O pins of the

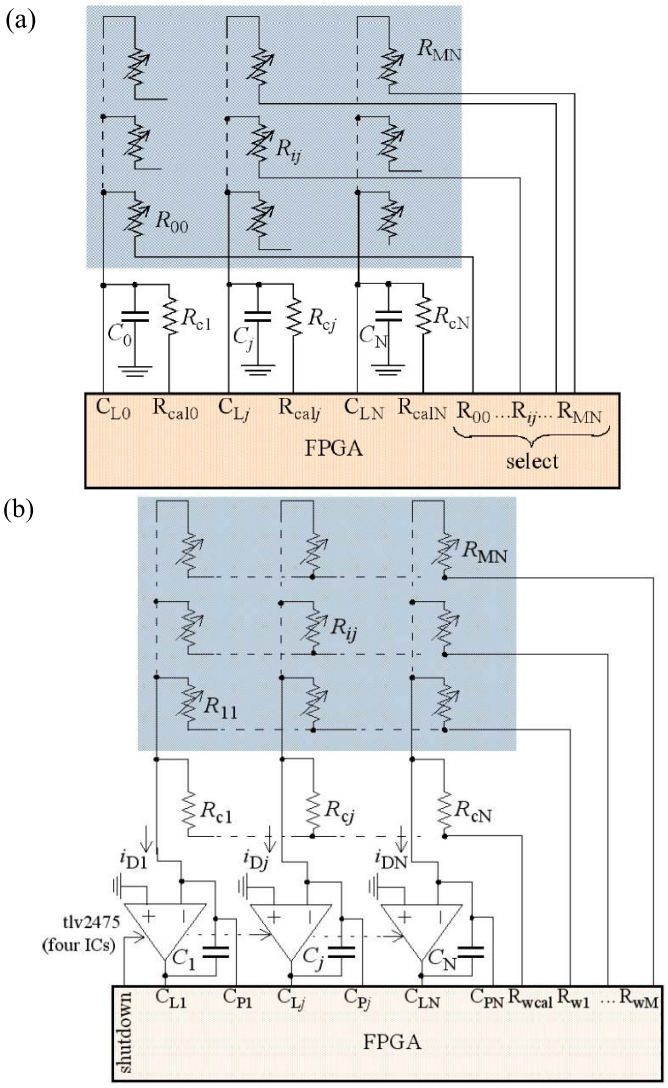

Fig. 3. (a) Schematic of an $M \times N$ sensor array with the PIM for low-medium size arrays (C_js are integrated capacitors, R_{cj}s are calibration resistors) [9]. (b) Schematic of an $M \times N$ sensor array with the PIM for large arrays (C_js are integrated capacitors) [9].

FPGA, every shared row wire was used as row selection wire and every shared column wire was connected to the shared node between the capacitor and the inverting input port of the op-amp. The PIM for large arrays was feasible for large-scale arrays for its requirement of $2 \times N + M$ pins in the $M \times N$ RSA, for example 48 pins in the 16×16 array. With the timers in the FPGA, the discharge time on C_j was measured synchronously and the EBT's resistance (R_{ij}, $i = 1$ to M, $j = 1$ to N) could be calculated with (4). Thus, sensor-digital conversion circuit with less cost and faster scanning rate was realized.

$$R_{ij} = \frac{V_{DD}}{(V_{DD} - V_{TL})C_j} t_{Dj} \quad (4)$$

where, t_{Dj} is the time measured by the timer, V_{DD} is the voltage across the capacitor at the beginning of the discharging phase, and V_{TL} is the low threshold voltage.

But accuracy and resistance range of the PIM were affected by many non-idealities such as the I/O pins' limited driving

capability of the FPGA, the op-amp's features including its offset voltage, its bias current, and its associated impedances, and the integral capacitor' feature including temperature coefficient and time stability. The application of the PIM is also limited by the electrodes' distributed capacitances, which are susceptible to be affected by electromagnetic noise. Better performance of the PIM could be realized by integrating the integral capacitors, the op-amps, and the time counters in an integrated analog-digital mixed-signal chip.

D. The Resistance Matrix Approach

The application of the RMA in the 2-D RSA as shown in Fig.4 [12] was proposed by Shu *et al.*, who determined sensor resistance values by establishing and solving resistance matrix equations of sensor arrays and realized a 10×10 tactile RSA with its scanning rate of 30 Hz and its measurement accuracy of $0.61 \pm 0.41\%$.

Without additional electrical components such as transistors, diodes, multiplexers, op-amps, switches, current sources, and A/D converters, wearable system based on the RMA with A/D converters and I/O ports embedded in a microcontroller had good performance such as low-cost, low-complexity [12]. The $M \times N$ RSA based on the RMA consists of one row of standard resistors (R_{sj}, $j = 1$ to N) and M rows of resistive elements (R_{ij}, $i = 1$ to M, $j = 1$ to N). To access sensor resistances (R_{ij}, $i = 1$ to M) on the jth column, $M + 1$ voltage combinations are sequentially allocated to I/O ports of the microcontroller (all row electrodes) to establish a matrix equation set (as shown in (5) [12]) whose solution refers to the sensor resistances. In every voltage combination, N voltages (V_{ij}, $j = 1$ to N) on all column electrodes (p_1 to p_N) were measured when the ith row electrode ($i = 1$ to $M + 1$) was connected to ground, and all other row electrodes except the ith row electrode were connected to V_{CC}.

$$\begin{bmatrix} R_{1j} \\ \vdots \\ R_{ij} \\ \vdots \\ R_{Mj} \end{bmatrix} = \begin{bmatrix} \frac{\frac{V_{2j}}{V_{cc}-V_{2j}}+1}{\frac{V_{1j}}{V_{cc}-V_{1j}}+1} R_{sj} \\ \vdots \\ \frac{\frac{V_{(i+1)j}}{V_{cc}-V_{(i+1)j}}+1}{\frac{V_{1j}}{V_{cc}-V_{1j}}+1} R_{sj} \\ \vdots \\ \frac{\frac{V_{(M+1)j}}{V_{cc}-V_{(M+1)j}}+1}{\frac{V_{1j}}{V_{cc}-V_{1j}}+1} R_{sj} \end{bmatrix} \tag{5}$$

In the RMA, a large amount of computations and 12-bit or higher (16-bit) ADCs were necessary for small resistance measurement error. In the real circuits, the I/O port's internal resistance was about tens of ohms and the voltages on row electrodes were neither precise V_{CC} (connected to V_{CC}) nor precise zero potential (connected to ground). Thus the RMA's ideal condition would be broken in the large-scale RSA.

E. The Incidence Matrix Approach

Federico *et al.* proposed the application of the IMA in the 2-D RSA [13]. As shown in Fig. 5 [12], with interconnections

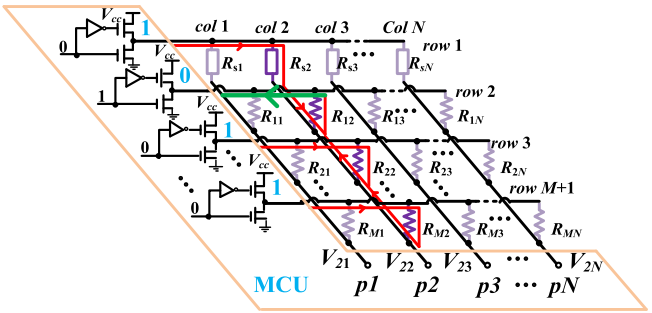

Fig. 4. Schematic of an $M \times N$ sensor array with the RMA (p_j pins are connected to I/O ports of the microcontroller, and V_{2j} is the voltage on the jth column with the second row electrode connected to ground and the other row electrodes connected to V_{CC}) [12].

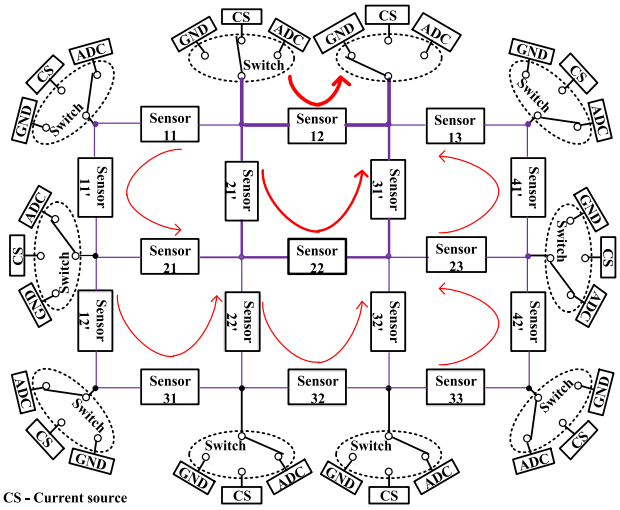

Fig. 5. Schematic of a sensor array with Incidence matrix approach ($sensor_{ij}$s and $sensor_{ij'}$s are resistive sensors in the array) [12].

placed between adjacent sensors, the IMA-based RSAs estimates the internal resistance distribution by taking injected current from the CS and potential measurements only at boundary, which is similar to the EIT [48].

Fundamental equations for the IMA in terms of the injecting current, incidence matrix, sensor resistance, and border voltage can be derived with by Kirchoff's and constitutive laws, and solved by a large number of computations to obtain the resistance of each sensor [12]. With similar features existed in the EIT, the application of the IMA was limited by its features including large number of computations, low spatial resolution, small resistance range, and low frequency response.

F. The Voltage Feedback Method

The application of the VFM in the 2-D force sensing resistor array was firstly described by Tise [14] who realized a 16×16 piezoresistive sensor array with its scanning rate of 10 Hz. He also pointed out that the scanning rate could be improved with more feedback resistors. With the VFM, Speeter [15], [16] realized a 16×16 tactile sensing system for robotic manipulation with a scanning rate of 60 Hz. Based on different connections of the feedback voltage with the

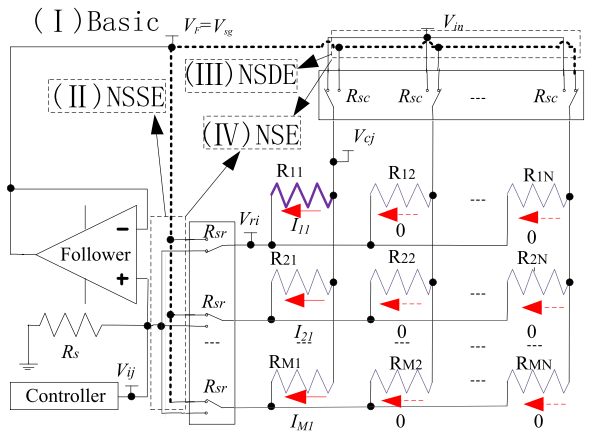

Fig. 6. Schematic of an $M \times N$ sensor array with the VFMs (V_{in} is the excitation voltage, R_s is the reference resistance, and V_F is the feedback voltage) [23].

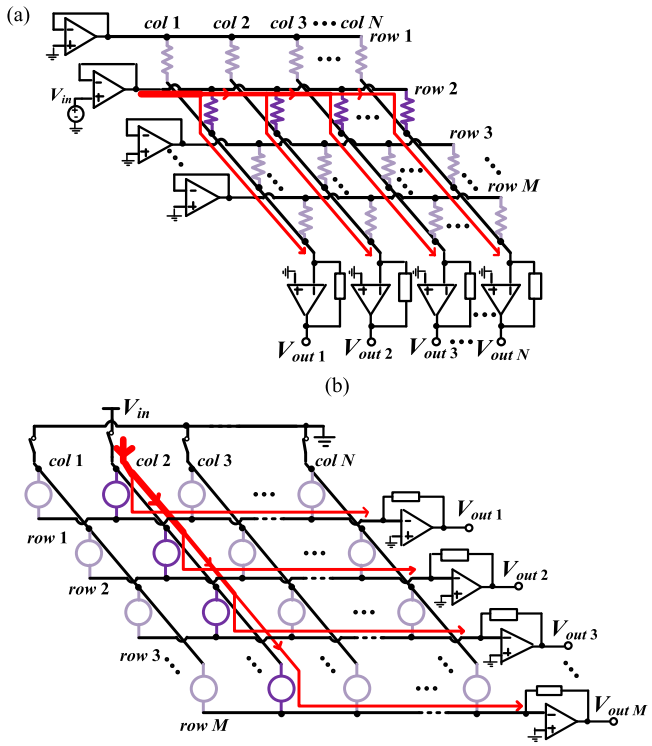

Fig. 7. (a) Schematic of an $M \times N$ sensor array with the ZPM based on the FVG technology (V_{in} is the excitation voltage, and V_{outi}s are the EBT's output voltages on the selected row) [24]. (b) Schematic of an $M \times N$ sensor array with the ZPM based on the PVG technology (V_{in} is the excitation voltage, and V_{outi}s are the EBT's output voltages on the selected column) [25].

sampling- electrode and the driving-electrode, Liu *et al.* [17] classified VFMs into the VF-NSE method, the VF-NSSE method, and the VF-NSDE method, and then evaluated their performances. D'Alessio [18] evaluated the measurement errors and power consumption of the circuits based on the VF-NSE method. The IDFC based on the VFM was implemented in the thermistor array [19]. For suppressing the crosstalk error caused by the multiplexers' switch-on resistances, more VFMs including the IIDFC [20] and the IIDFCC [21] were proposed and their performances were evaluated. With low readout rate for using only one sampling op-amp and two sampling channels, cable crosstalk of long cable was well suppressed by the two-wire VFM method using two wires for both every driving electrode and every sampling electrode [22].

As shown in Fig.6 [23], shared column wires and shared row wires were used as driving electrodes and sampling electrodes respectively. In the VFM, with output voltage feeding back to column wires and row wires through a low output impedance op-amp, the voltage drop of every element on all non-scanned columns was very small and the bypass currents on all non-scanned elements were significantly reduced. Thus the EBT's resistance in the VFM could be determined by isolating the EBT from the array. In the VF-NSSE method, the feedback voltage drove the non-scanned-sampling electrodes. In the VF-NSDE method, the feedback voltage drove the non-scanned-driving electrodes. In the VF-NSE method, the feedback voltage drove all non-scanned electrodes. In the VFM with minimum circuitry, only one element could be tested at the same time with its output voltage feeding back to the electrodes of the array, which led to the low scanning rates of the VFMs. By measuring the voltage (V_{ij}, $i = 1$ to M, $j = 1$ to N) on the sampling resistor (R_s), the EBT's resistance (R_{ij}, $i = 1$ to M, $j = 1$ to N) could be calculated with (6) in the VFMs.

$$R_{ij} = \frac{V_{in} - V_{ij}}{V_{ij}} R_s \tag{6}$$

As parasitic parallel currents on the non-scanned elements would increase with the increase of array size and the decrease of the non-scanned element' resistance, the measurement errors of the VFMs were significantly affected by the RSA's array size and the EBT's resistance range. At the same time, parasitic parallel currents could interfere in the EBT's test current path with the multiplexers' switch-on resistances, the sampling resistance, and wire resistances and contacted resistances of the connected cables. Non-ideal parameters of the op-amp could cause a difference between the feedback voltage and the sampling voltage. Thus, the measurement errors of the VFMs were affected by the circuits' parameters including the multiplexers' switch-on resistances, the sampling resistance, the op-amps' features, and wire resistances and contacted resistances of the connected cables. The saturation of the op-amp occurred less in the VFM, which had a varied resolution throughout the measurement range caused by its nonlinear relation between the output voltage and the EBT's resistance. Thus, the VFM would have a wide resistance range limited by the circuit noise and the ADC's conversion accuracy.

G. Zero Potential Method

The application of the ZPM [24] (Fig.7(a)) was firstly described by Lazzarini *et al.*, who determined the resistance values by isolating the elements on the same row from the 2-D RSA using the FVG technology with large number of op-amps and realized a scanning rate of 200 Hz on the 16 × 16 piezoresistive sensor array with the tested cable's

length of 500 mm. With many sampling op-amps and less driving op-amps, the crosstalk caused by the row adjacent elements was suppressed by the PVG-based ZPM [25] (Fig.7(b)) with a high readout rate. By connected to virtual ground with driving op-amps or by directly connected to ground through the multiplexers, all non-scanned driving-electrodes in the ZPMs had zero potential. All scanned sampling-electrodes had zero potential with all sampling op-amps in negative feedback. Therefore, the voltage drop on every non-scanned element was very small and the bypass currents on all non-scanned elements were significantly reduced. Thus the EBT's resistance in the ZPMs could be determined by isolating the EBT from the array.

In the large-scale RSA based on the ZPM, the crosstalk error caused by the input offset voltage and the input bias current of the op-amp was well suppressed by the double-sampling technique [26], which were significant in the large-scale RSAs with elements of large resistance value. With low readout rate for using only one sampling op-amp and two sampling channels, cable crosstalk of long cable was well suppressed by the two-wire method using two wires for both every driving electrode and every sampling electrode [27]. With high readout rate for using many sampling op-amps, cable crosstalk for long cables was partly suppressed by the part two-wire method using two wires for every driving electrode but one wire for every sampling electrode [28]. With high readout rate for using many sampling op-amps, cable crosstalk for long cables was completely suppressed by the full two-wire method using two wires for every driving electrode and every sampling electrode [29]. As the drop voltages on wire resistance and the multiplexer's switch-on resistance were eliminated by these two-wire methods, better results were achieved.

As shown in Fig.8, ZPMs [17] using one op-amp were classified into the S-NSE-ZP method, the S-NSSE-ZP method, and the S-NSDE-ZP method. In the S-NSSE-ZP method, ground was connected with the non-scanned-sampling multiplexers and the non-scanned-sampling electrodes were set at zero potential. In the S-NSDE-ZP method, ground was connected with the non-scanned-driving multiplexers and the non-scanned-driving electrodes were set at zero potential. In the S-NSE-ZP method, ground was connected with all non-scanned multiplexers and all non-scanned electrodes were set at zero potential. In some circuits [9], [28], the reference voltages were not zero potential, so op-amps and ADCs with unipolar power sources could be conveniently used with less cost. So Wu and Wang [27] defined the S-NSE-EP method, the S-NSSE-EP method, and the S-NSDE-EP method.

In Fig.8 [30], R_{11} was the EBT, column wires and row wires were used as driving electrodes or sampling electrodes.

As "virtual short" and "virtual-off" occurred between the inverting ports and the non-inverting ports of the op-amps, the current on every non-scanned element in the ZPM was zero potential for two terminals of every non-scanned element were equipotential. Thus the test current only passed through the EBT (R_{xy}, $x = 1$ to M, $y = 1$ to N) and its sampling resistor, the crosstalk caused by non-scanned elements was eliminated with the ZPM and the EBT's resistance value was determined.

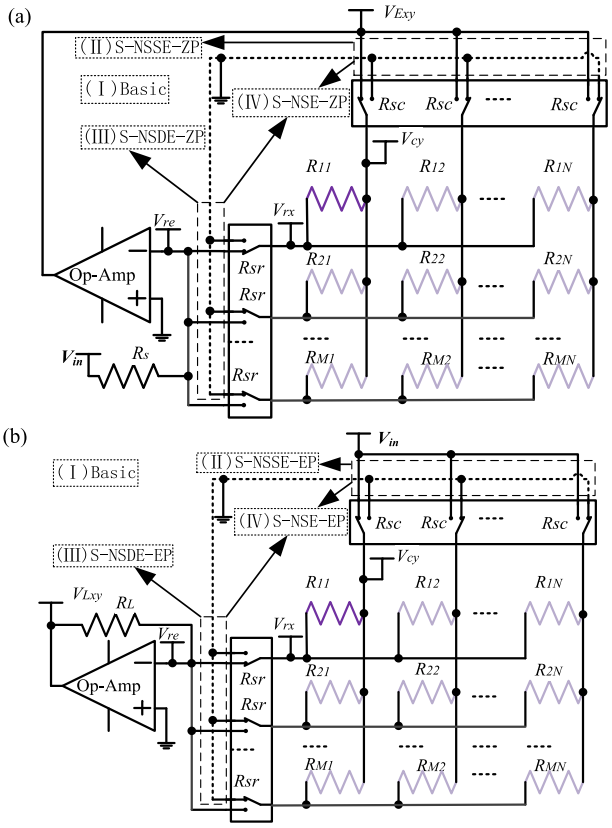

Fig. 8. (a) Schematic of an $M \times N$ sensor array with the ZPMs with the EBT as the feedback resistor (V_{in} is the excitation voltage, and V_{Exy} is the EBT's output voltage) [30]. (b) Schematic of an $M \times N$ sensor array with the ZPMs with the standard resistor as the feedback resistor (V_{in} is the excitation voltage, and V_{Lxy} is the EBT's output voltage) [30].

In Fig.8 (a), a standard resistor (R_s) and the EBT were used as the resistor to preset the tested current and a feedback resistor respectively, in which the EBT's resistance had a linear relation with its output voltage (V_{Exy}, $x = 1$ to M, $y = 1$ to N) as shown in (7). In Fig.8 (b), the standard resistor (R_L) was used as the feedback resistor, in which the EBT's resistance had a non-linear relation with the output voltage (V_{Lxy}, $x = 1$ to M, $y = 1$ to N) as shown in (8). In Fig.7, many R_ss were used to synchronously sample the currents of the resistive elements on the same column, each with a negative feedback op-amp and a non-linear output voltage.

$$R_{xy} = -\frac{V_{Lxy}}{V_{in}} R_L \tag{7}$$

$$R_{xy} = -\frac{V_{in}}{V_{Exy}} R_s \tag{8}$$

As all elements on the same column or the same row in the RSA could be measured simultaneously by using many sampling op-amps in the ZPMs, which were widely used in many applications for their high readout rates. But the measurement ranges of the ZPMs were also susceptible to be limited by the saturation of the op-amp's output voltage.

Some typical kinds of scanning approaches' performances and characteristics are listed in Table 1.

TABLE I
COMPARISON OF DIFFERENT SCANNING APPROACHES OF THE $M \times N$ NETWORKED RESISTIVE SENSOR ARRAYS

Methods	Auxiliary components	Advantages	Disadvantages
IDM	$M \times N$ Diodes, N multiplexers, M sampling resistors and N channels of ADC	Fastest readout rate, large resistance range, low crosstalk between sensors	Normal accuracy, Complexity interconnection
ITM	$M \times N$ transistors, M multiplexers, N sampling resistors and N channels of ADC	Fastest readout rate, large resistance range, low crosstalk between sensors	Normal accuracy, Complexity interconnection
RMA	N standard resistors, N channels of ADC embedded in MCU	Faster readout rate, low complexity	Small array size, normal accuracy with 10-bit ADCs, large computation, limited resistance range
IMA	Inject current source	Measure only at boundary	Small array size, normal accuracy, large computation, low spatial resolution, low temporal frequency
PIM	N capacitors and N op-amps, FPGA with a large number of input/output ports	Fastest readout rate, resistance-digital conversion without independent ADCs	Capacitive coupled noise, limited resistance range
VFM*	One op-amp and one sampling resistor, $M + N$ multiplexers, one channel of ADC	Good accuracy, low cost, large resistance range, low interconnection complexity	Low scanning speed, Nonlinearity
ZPM with one op-amp*	One op-amp and one sampling resistor, $M + N$ multiplexers, one channel of ADC	Good accuracy, low cost, Low interconnection complexity	Low scanning speed, Limited resistance range
ZPM based on PVG*	N multiplexers, M sampling resistors, and M channels of ADC	Fastest readout rate, better accuracy, Low interconnection complexity,	Complexity circuit, Limited resistance range
ZPM based on FVG*	N multiplexers, M sampling resistors, and M channels of ADC	Fastest readout rate, Best accuracy, Low interconnection complexity,	Complexity circuit Limited resistance range

*One-wire method. With more wires, better accuracy could be obtained with the two-wire methods [22, 27-29].

III. ANALYSIS METHODS OF SCANNING APPROACHES IN RSAs

Different analysis methods such as testing of the actual system [9], [43], analyzing with circuit simulation software [17], [18], [25], [44]–[46], [49], and analyzing with test model [9], [20], [23]–[25], [30], [44], [46], [49]–[51], were used to evaluate the scanning approaches' performances in RSAs.

A. Testing of the Actual System

Three actual circuits [9] based on standard microcontrollers, Programmable Systems on Chip, and FPGAs respectively, were realized and evaluated for piezoresistive tactile sensors. Three actual circuits [43] including a symmetric resistive voltage division circuit, a symmetric resistive charge division circuit, and a charge division multiplexing resistor network circuit, were realized for investigating their behaviors in the flexible SensL's silicon photomultiplier array photo detector. At the cost of a large amount of manual work and material costs, the actual performances of RSAs and their scanning approaches could be thoroughly evaluated with the actual systems.

B. Analyzing With Circuit Simulation Software

In some literatures, performances of RSAs and their scanning approaches were analyzed with the circuit simulation software such as Cadence-Spectre, PSpice, NI Multisim, *etc*. Power consumptions and measurement errors of the scanning approaches in RSAs were evaluated with Montecarlo simulations [18]. Readout circuits of RSAs were evaluated with Cadence-Spectre [44]. With PSpice, Liu *et al.* [17] compared measurement errors of the VFCs and the ZPCs., Performances of readout circuits of RSAs and the noise's effect was evaluated with PSpice [25], [45], [46], [49].

Circuit simulation software was proved to be effective in analyzing the readout circuit's factors such as power consumption, error sources, and their weight coefficient in overall errors. With the parameters selected correctly, the simulation results were believable. But in circuit simulation software, lines and parameters of every device should be connected and preset respectively in every simulation, which would consume a large amount of manual work. Thus precise quantization error analysis of various factors was still difficult to realize for the circuit simulation software.

C. Analyzing With Test Model

Saxena *et al.* presented a concise test model as shown in Fig.9 [44] for the novel ZPM with one op-amp of the $N \times M$ RSA. In the test model, the EBT connected the inverting input port of the op-amp to the output port of the op-amp and the non-inverting input port of the op-amp connected to ground; $(N-1)$ row elements of selected column connected the inverting input port of the op-amp to ground; $(M-1)$ column elements of selected row connected the output port of the op-amp to ground; all terminals of rest $(N-1) \times (M-1)$ elements were connected to ground. With the test model, a ratio of the EBT's sensitivity to the row adjacent elements' sensitivity was given by theoretical deduction and analysis, which could be used to evaluate parameters including array size, resistances of

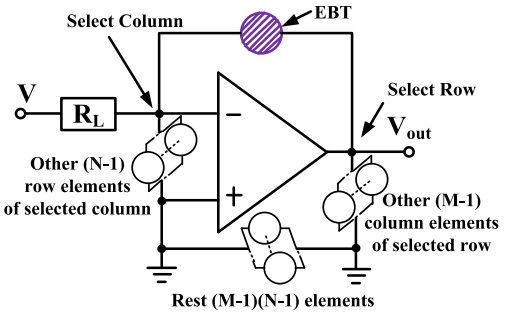

Fig. 9. The test model of the ZPM with one op-amp [44].

row adjacent elements, and the op-amp's gain. But in the test model, the multiplexers' switch-on resistances were neglected and their effect could not be analyzed.

By analyzing the distribution of bias current in the 2-D RSA, the approximate expression of the EBT's equal resistance change ($\Delta R_{1,1}^{eq}$) as shown in (9) [46] caused by small resistance variations (r_{ij}, $i = 1$ to N, $j = 1$ to N) of resistive elements (R_{ij}, $i = 1$ to N, $j = 1$ to N) in the $N \times N$ RSA and the approximate expression of the EBT's voltage change (V_{11}) as shown in (10) [49] caused by small resistance variations (r_{ij}, $i = 1$ to M, $j = 1$ to N) of resistive elements (R_{ij}, $i = 1$ to M, $j = 1$ to N) in the $M \times N$ RSA were given. Also the similar weight coefficient matrices and a crosstalk matrix representing the total crosstalk among various elements [49] were derived mathematically. But achieving the solution of crosstalk and snapshot capability simultaneously was proved to be difficult [50].

$$\Delta R_{1,1}^{eq} = K\left\{(2N-1)^2 r_{11} + (N-1)^2 \sum_{i=2}^{N} r_{1i} + (N-1)^2 \sum_{i=2}^{N} r_{i1} + \sum_{i=2}^{N}\sum_{j=2}^{N} r_{ij}\right\} \quad (9)$$

$$V_{11} = K\left[(N+M+1) r_{11} + N \sum_{j=2}^{M} r_{1j} + M \sum_{i=2}^{N} r_{i1} - \sum_{i=2}^{N}\sum_{j=2}^{M} r_{ij}\right] \quad (10)$$

In the circuit model of the part virtual ground ZPM using many sampling op-amps [25], practical non-idealities and limitations were discussed, the expressions for sensitivity and crosstalk rejection were derived, and suggestions to reduce the overall noise and crosstalk were given.

A mathematical voltage expression (V_s) of the EBT (R_{xy}, $x = 1$ to M, $y = 1$ to N) as shown in (11) [51] and a mathematical equivalent resistance (R_{eq}) of the EBT as shown in (12) [51] for the VF-NSE method in the $M \times N$ RSA were analytically derived. The expressions of the EBT were proved to be affected by the sampling resistance (R_s), the row multiplexer's switch-on resistances (R_rs), the column multiplexer's switch-on resistances (R_cs), the column adjacent

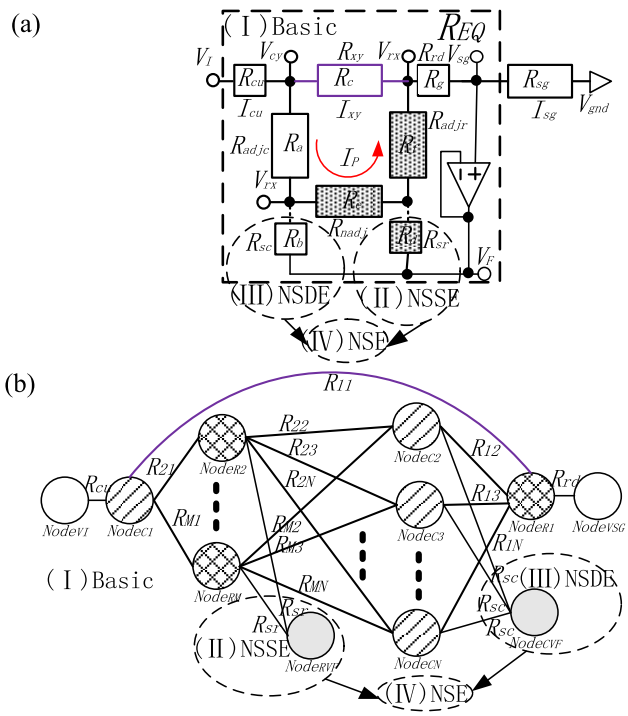

Fig. 10. (a) General approximate circuit model of VFCs [24]. (b) Topological structures of VFCs [24].

TABLE II
PARAMETERS OF CIRCUIT MODEL IN FIG.10(A) [23]

	Basic	VF-NSSE	VF-NSDE	VF-NSE
R_a			$R_{adjr}/(M-1)$	
R_b	∞	$R_{sr}/(M-1)$	∞	$R_{sr}/(M-1)$
R_c			R_{xy}	
R_d	∞	∞	$R_{sc}/(N-1)$	$R_{sc}/(N-1)$
R_e			$R_{nadj}/(M-1)/(N-1)$	
R_f			$R_{adjc}/(N-1)$	
R_g			R_{rd}	

elements (R_{my}s), and the row adjacent elements (R_{xn}s).

$$V_s = \frac{R_c + K_y R_r + K_x R_c + K_y(1+K_x) R_{xy}}{R_c + R_s + K_y R_r + K_x R_c + K_y(1+K_x) R_{xy}} V_I \quad (11)$$

$$R_{eq} = \frac{(R_c + K_y R_r + K_x R_c)(V_F - V_I) + R_s V_F}{K_y(1+K_x)(V_I - V_F)} \quad (12)$$

where, $K_x = \sum_{n=1\ \&\ n\neq y}^{N} \frac{R_r}{R_{xn}}$, $K_y = 1 + \sum_{m=1\ \&\ m\neq x}^{M} \frac{R_c}{R_{my}}$ $K_y = 1 + \sum_{m=1\ \&\ m\neq x}^{M} \frac{R_c}{R_{my}}$, the V_F is the EBT's feedback voltage, and the V_I is the excitation voltage.

A mathematical expression of the equivalent resistance (R_{eq}) of the EBT (R_{xy}, $x = 1$ to M, $y = 1$ to N) for the IIDFC of the $M \times N$ RSA as shown in (13) [20] was analytically derived, which was proved to be effective in fast evaluating the effect of different parameters such as R_r, R_c, M, N, and R_{my}s.

$$R_{eq} = R_c + R_r + R_{xy}\left(1 + \sum_{m=1\ \&\ m\neq x}^{M} \frac{R_c}{R_{my}}\right) \quad (13)$$

TABLE III
COMPARISON OF DIFFERENT ANALYSIS METHODS FOR THE SCANNING APPROACHES IN THE RESISTIVE SENSOR ARRAYS

Methods	Reliable	Fast	Cost	Suitable to
Testing of the actual system	***	-	-	All scanning approaches and their actual systems
Analyzing with circuit simulation software	**	*	*	All scanning approaches and their simulation circuits
analyzing with test model	*	***	***	PIM, VFM, ZPM

'-': normal;'*': good; '**': better; '***':best.

For analyzing the performances of three VFCs, a general approximate circuit model (Fig.10 (a)), its topological structure (Fig.10 (b)), and its R_{eq}'s mathematical expression were presented in [23]. Parameters in the VFCs' model were shown in Table 2 [23]. Similar model and its R_{eq}'s expression were proposed for analyzing the performances of the ZPCs [30]. These expressions were proved to be effective in fast evaluating these circuits' performance of parameters such as the multiplexers' switch-on resistances, the non-scanned elements, and array size. But these expressions were not concise.

In the PIM, a new calibration model of the direct RSA to FPGA interface was proposed to eliminate the uncertainty caused by RC crosstalk [9].

With adequate understanding of their working mechanisms, the accurate models of the scanning approaches in the RSAs could be achieved. Mathematical expression of the EBT's R_{eq}, which was useful for fast analyzing the performance of different parameters in the array and its circuit, could be analytically derived with the accurate model.

Performances and applications of some typical kinds of analysis methods for scanning approaches in the 2-D RSAs are listed in Table 3.

IV. APPLICATIONS OF SCANNING APPROACHES IN RSAS

As scanning approaches improve, RSAs will see wide application in the fields of tactile sensor, electronic skin, imaging sensor, chemical sensor, and human-machine interaction input device.

A. Tactile Sensor and Electronic Skin

With the transducer as a resistor sensitive to pressure or strain, different RSAs were applied in tactile sensor and electronic skin which were useful for haptically exploring objects and environments, detecting features, recognizing objects, localizing objects, and estimating object properties. In them, different scanning approaches including the IDM [2], [3], the ITM [8], the PIM [9], the RMA [12], the IMA [13], the VFM [14], [15], and the ZPM [31]–[38], were applied.

With the ZPM, Kim *et al.* realized a 5 × 5 resistive tactile sensor array [31] with semiconductor strain gages; Vidal-Verdú *et al.* [32] developed a 16 × 9 resistive tactile sensor patch to cover large areas of robots and machines that interacted with human beings; Luo and Jiang [33] developed a 16 × 16 flexible RSA with spatial resolution of 1 mm and realized a scanning rate of 1.2 kHz; Yang *et al.* [34], Cheng *et al.* [35], Yang *et al.*[36], Shih *et al.* [37], and Cheng *et al.* [38] designed the artificial skin having a 32 × 32 thermistors and tactile sensing flexible array [34] within the 160 mm × 160 mm sensing area and realized a scanning rate of 3,000 elements per second.

More RSAs with better performances including ultra-sensitive pressure [52], full surface coverage [53], [54], in vivo detection [55], and large elongation [56], were developed, which put forward many special requirements such as large array size, fast readout rate, large resistance range, good accuracy, low complexity, scalability, flexibility, and stretchability on the scanning approaches of RSAs.

B. Imaging Sensor

With photoresistor [5], [44], resistive bolometer [45], [46], and thermistor [47], imaging sensors were widely used in detection of light, thermal radiation, and electron radiation. Large array size (e.g. 128 × 128 in [5]), high accuracy and fast readout rate of imaging sensor are still challenges for most readout circuits of large-scale RSAs.

C. Chemical Sensor

Based on the VFM, an electronic scanning system with a polymeric chemical sensor array consisting of 65536 resistive sensors comprising tens of different types was realized by Beccherelli *et al.* [39]. Using resistance-to-number conversion with the oscillator, Conso *et al*. [40] realized an 8-bit accuracy, 6-decades- range gas sensor interface chip with the capability of handling a 5 × 5 sensor matrix. Large array size, large resistance range, and multi-type of chemical sensors are still challenges for most readout circuits of large-scale RSAs.

D. Human-Machine Interaction Input Device

With the VFM, recognizing of handwritten digit characters was realized by Wang *et al*. [41] and Wu *et al.* [42] with the handwritten input device of an 8 × 16 thermistor array. For good performance of human-machine interaction input devices with RSAs, scanning approaches with large array size, high accuracy and fast readout rate are necessary.

Similar readout circuits were also used in RRAM [57], [58] based on the resistive switching phenomenon. The array size of RRAM could be 1024 × 1024 [58] and wire resistance within the crossbar was found to be an outstanding challenge [57]. Wire resistances between elements in RSAs with small array size were small and they were neglected in most readout

TABLE IV
SPECIAL REQUIREMENT ON SCANNING APPROACHES IN EACH APPLICATION

Application	Scanning approach	Special requirements
Tactile sensing, Electronic skin	IDM, ITM, PIM, RMA, IMA, VFM, ZPM	Scalability, Flexibility, Stretchability, Large array size, Fast readout rate, Wide range, Good accuracy, Low complexity
Chemical sensor	VFM, resistance-to-number	Large array size, Wide range, Good accuracy
Man-machine interaction input device	IDM, ITM, VFM, ZPM	Scalability, Flexibility, Stretchability, Large array size, Fast readout rate, Low complexity
Imaging of light / thermal / electron radiation	IDM, ITM, ZPM	Fast readout rate, Low complexity, Easy to integration

circuits for now. As large resistivity wire with flexible feature would be used in RSAs with large scale, long wire could cause large wire resistance which would significantly affect the readout circuits' performance. Thus, wire resistance's effects on scanning approaches should be analyzed in future work.

These applications put forward many special requirements on RSAs and their scanning approaches as shown in Table 4.

V. DISCUSSION AND CONCLUSION

Scanning approaches are very important for the 2-D RSA and the 3-D RSAs [4], [59]. After fabrication of one integrated sensor with many resistive sensitive elements arranged in array within a package, the connection and the topological structure of the sensitive elements are fixed, and the selection of its scanning approaches and its measurement accuracy of the physical parameters distributed in a certain area are limited. Thus research of the scanning approach is very important for improving the performance of the resistive sensor. As for the RSA with many discrete resistive sensors, its interconnection and the topological structure of the sensitive elements in the scanning approach can be determined according to actual requirements. A good scanning approach can ensure both measurement accuracy and scanning rate of all elements in the array, also it can make it possible for the RSAs with a larger array size, a larger resistance range, more choices of auxiliary circuit components (*e.g.* multiplexers with different switch-on resistances), and better sensing systems with lower cost and lower power consumption. Many scanning approaches were used in different sensing applications. In these approaches, the ITM, the IDM, the PIM, the RMA, and the ZPM with many sampling op-amps have the fast readout rate; the PIM and the RMA have low-complexity; the IDM, the ITM and the ZPM the ZPM with many sampling op-amps have large capacity of sensitive elements; the IDM and the ITM are ease of integration; the VFM and the ZPM have high precision. Each scanning approach had its application situation and it should be selected according the special requirements in the applications.

A. Measurement Accuracy

Measurement accuracy of the RSA is affected by both conversion accuracy of the physical parameter into resistance in the sensitive element and the RSA's scanning approach. Conversion accuracy of the sensitive element depends on its conversion mechanism and fabrication technology. Under the condition that the sensitive element can accurately and linearly convert the physical parameter to its resistance, measurement accuracy of the sensor depends on the actual readout circuit. Measurement accuracy of the actual readout circuit is affected by the RSA's parameters and the circuits' parameters.

Measurement accuracy of the existing scanning approaches of RSAs is challenged by many factors such as wider resistance range of the chemical sensor array, larger scale of the image sensor, long flexible test cable existing in the tactile sensor, and flexibility, stretchability, large area, and multi-function in the artificial electronic skin.

B. Readout Rate

Fast readout rate is still a challenge for most readout circuits of large-scale RSAs, which is affected by frequency response characteristics of their sensitive elements and their readout circuits. The response speed of the readout circuit should be significantly faster than that of the sensitive element responding to external physical excitation.

With many sampling op-amps and parallel analog-to-digital conversions, fast readout circuits including the ZPCs and the passive integrator circuits could accurately readout the resistances of the elements on the same column or the same row in the RSA. But these fast readout circuits with complex structures also had large power consumption and high cost.

C. Array Size, Covering Area, and Spatial Resolution

In tactile sensing applications, both larger overall sensing area (covering area) and higher spatial resolution are hoped to be obtained. Spatial resolution is determined by the sensing area of each element (pixel area) and the spacing between two adjacent elements in the RSA. But array size, covering area, and spatial resolution are influenced mutually. The less the covering area is and the larger the array size is, the higher the spatial resolution is, and vice versa. With certain covering area, the larger the array size is, the higher the spatial resolution is and the more the positioning accuracy of the contact location is. Larger covering area can introduce more space electromagnetic interference, which will lead to extra error in scanning approach. With larger array size, more elements exist in the RSA, which will require larger driving ability of the op-amp, consume more power, and cause more significantly crosstalk problem for larger bypass current.

Support capability of the scanning approach on large array size and large area is still challenged by sensing applications including the large-scale imaging sensor and the flexible, stretchable, large area, and multi-function electronic skin.

D. Flexibility

Wearable, flexible sensor including artificial electronic skin and tactile sensor put forward new requirement that readout circuits should not change the flexibility of the RSA and its adjacent regions. Flexible circuit boards and long flexible test cables were good choices, but which would also lead to adverse factors such as mechanical vibration, cable resistance, interface resistance, *etc*.

E. Large Resistance Range

With more functions in the RSA, scanning approach needed to measure sensitive elements with different resistance ranges. Thus scanning approaches with wide resistance range are necessary for RSAs used in tactile sensor and chemical sensor. New scanning approaches, for example resistance-to-number conversion with the oscillator, should be developed for the RSA with the large resistance range.

F. Analyzing Method of Scanning Approaches in RSAs

As stated above, testing of the actual system, analyzing with circuit simulation software, and analyzing with test model were used to evaluate the performance of RSAs and their scanning approaches. At the cost of a large amount of manual work and material costs, comprehensive, real and reliable results could be obtained with testing of the actual system. With the advantage of low material costs but the disadvantage of a large amount of manual work, relatively reliable results could be obtained by analyzing the scanning approaches in the RSAs with circuit simulation software. At the primary stage of development, test models and their mathematical expressions of the scanning approaches in RSAs at low costs were more preferred for fast analyzing their features and selecting their optimal parameters. Thus, mechanism research on test models of the scanning approaches is still very important for the applications of RSAs.

REFERENCES

[1] D. Goger and H. Worn, "A highly versatile and robust tactile sensing system," in *Proc. IEEE SENSORS*, Oct. 2007, pp. 1056–1059.

[2] W. E. Snyder and J. S. Clair, "Conductive elastomers as sensor for industrial parts handling equipment," *IEEE Trans. Instrum. Meas.*, vol. 27, no. 1, pp. 94–99, Mar. 1978.

[3] D. Prutchi and M. Arcan, "Dynamic contact stress analysis using a compliant sensor array," *Measurement*, vol. 11, no. 3, pp. 197–210, 1993.

[4] J. X. Ding, "Study on some problems of a kind of 3-D flexible tactile sensor arrays based on ideal flow-forming conductive rubber," Ph.D. dissertation, Dept. Automa., Univ. Sci. Technol. China, Hefei, China, 2011.

[5] A. Tanakaet *et al.*, "Infrared focal plane array incorporating silicon IC process compatible bolometer," *IEEE Trans. Electron. Devices*, vol. 43, no. 11, pp. 1844–1850, Nov. 1996.

[6] K. Takei *et al.*, "Nanowire active-matrix circuitry for low-voltage macroscale artificial skin," *Nature Mater.*, vol. 9, no. 10, pp. 821–826, 2010.

[7] C. Wang *et al.*, "User-interactive electronic skin for instantaneous pressure visualization," *Nature Mater.*, vol. 12, no. 10, pp. 899–904, 2013.

[8] B. J. Kane, M. R. Cutkosky, and G. T. A. Kovacs, "A traction stress sensor array for use in high-resolution robotic tactile imaging," *J. Microelectromech. Syst.*, vol. 9, no. 4, pp. 425–434, Dec. 2000.

[9] F. Vidal-Verdú, Ó. Oballe-Peinado, J. A. Sánchez-Durán, J. Castellanos-Ramos, and R. Navas-González, "Three realizations and comparison of hardware for piezoresistive tactile sensors," *Sensors*, vol. 11, no. 3, pp. 3249–3266, 2011,.

[10] Ó. Balle-Peinado, F. Vidal-Verdú, J. A. Sánchez-Durán, J. Castellanos-Ramos, and J. A. Hidalgo-López, "Accuracy and resolution analysis of a direct resistive sensor array to FPGA interface," *Sensors*, vol. 16, no. 2, p. 181, 2016.

[11] Ó. Balle-Peinado, F. Vidal-Verdú, J. A. Sánchez-Durán, J. Castellanos-Ramos, and J. A. Hidalgo-López,, "Improved circuits with capacitive feedback for readout resistive sensor arrays," *Sensors*, vol. 16, no. 2, p. 149, 2016.

[12] L. Shu, X. Tao, and D. D. Feng, "A new approach for readout of resistive sensor arrays for wearable electronic applications," *IEEE Sensors J.*, vol. 15, no. 1, pp. 442–452, Jan. 2015.

[13] F. Lorussi, W. Rocchia, E. P. Scilingo, A. Tognetti, and D. D. Rossi, "Wearable, redundant fabric-based sensor arrays for reconstruction of body segment posture," *IEEE Sensors J.*, vol. 4, no. 6, pp. 807–818, Dec. 2004.

[14] B. Tise, "A compact high resolution piezoresistive digital tactile sensor," in *Proc. IEEE Int. Conf. Robot. Autom.*, New York, NY, USA, Apr. 1988, pp. 760–764.

[15] T. H. Speeter, "Flexible, piezoresitive touch sensing array," *Proc. SPIE*, vol. 1005, pp. 31–43, Mar. 1989.

[16] T. H. Speeter, "A tactile sensing system for robotic manipulation," *Int. J. Robot. Res.*, vol. 9, no. 6, pp. 25–36, 1990.

[17] H. Liu, Y.-F. Zhang, Y.-W. Liu, and M.-H. Jin, "Measurement errors in the scanning of resistive sensor arrays," *Sens. Actuators A, Phys.*, vol. 163, no. 1, pp. 198–204, 2010.

[18] T. D'Alessio, "Measurement errors in the scanning of piezoresistive sensors arrays," *Sens. Actuators A, Phys.*, vol. 72, no. 1, pp. 71–76, 1999.

[19] J. Wu, L. Wang, J. Li, and Z. Yu, "A small size device using temperature sensor array," *Chin. J. Sens. Actuat.*, vol. 24, no. 11, pp. 1649–1652, 2011.

[20] J. Wu, L. Wang, and J. Li, "Design and crosstalk error analysis of the circuit for the 2-D networked resistive sensor array," *IEEE Sensors J.*, vol. 15, no. 2, pp. 1020–1026, Feb. 2015.

[21] J. Wu, L. Wang, J. Li, and A. Song, "A novel crosstalk suppression method of the 2-D networked resistive sensor array," *Sensors*, vol. 14, no. 7, pp. 12816–12827, 2014.

[22] J. Wu, S. He, J. Li, and A. Song, "Cable crosstalk suppression with two-wire voltage feedback method for resistive sensor array," *Sensors*, vol. 16, no. 2, p. 253, 2016.

[23] J. Wu, L. Wang, and J. Li, "General voltage feedback circuit model in the two-dimensional networked resistive sensor array," *J. Sensors*, vol. 2015, Jun. 2015, Art. no. 913828

[24] R. Lazzarini, R. Magni, and P. Dario, "A tactile array sensor layered in an artificial skin," in *Proc. IEEE/RSJ Int. Conf. Intell. Robot. Syst. Human Robot Interact. Cooperat. Robot.*, vol. 3, Aug. 1995, pp. 114–119.

[25] R. S. Saxena, R. K. Bhan, N. K. Saini, and R. Muralidharan, "Virtual ground technique for crosstalk suppression in networked resistive sensors," *IEEE Sensors J.*, vol. 11, no. 2, pp. 432–433, Feb. 2011.

[26] R. Yarahmadi, A. Safarpour, and R. Lotfi, "An improved-accuracy approach for readout of large-array resistive sensors," *IEEE Sensors J.*, vol. 16, no. 1, pp. 210–215, Jan. 2016.

[27] J. Wu and L. Wang, "Cable crosstalk suppression in resistive sensor array with 2-wire S-NSDE-EP method," *J. Sensors*, vol. 2016, Feb. 2016, Art. no. 8051945.

[28] J. S. Kim, D. Y. Kwon, and B. D. Choi, "High-accuracy, compact scanning method and circuit for resistive sensor arrays," *Sensors*, vol. 16, no. 2, p. 155, 2016.

[29] J. Wu *et al.*, "A novel two-wire fast readout approach for suppressing cable crosstalk in a tactile resistive sensor array," *Sensors*, vol. 16, no. 5, p. 720, 2016.

[30] J. Wu and J. Li, "Approximate model of zero potential circuits for the 2-D networked resistive sensor array," *IEEE Sensors J.*, vol. 16, no. 9, pp. 3084–3090, May 2016.

[31] M.-S. Kim, H.-J. Shin, and Y.-K. Park, "Design concept of high-performance flexible tactile sensors with a robust structure," *Int. J. Precis. Eng. Manuf.*, vol. 13, no. 11, pp. 1941–1947, 2012.

[32] F. Vidal-Verdú *et al.*, "A large area tactile sensor patch based on commercial force sensors," *Sensors*, vol. 11, no. 5, pp. 5489–5507, 2011.

[33] Z. Z. Luo and J. P. Jiang, "A high resolution and flexible piezoresistive tactile sensor array," *J. Zhejiang Univ. Eng. Sci.*, vol. 33, no. 6, pp. 569–573, 1999.

[34] Y.-J. Yang *et al.*, "A 32 × 32 temperature and tactile sensing array using PI-copper films," *Int. J. Adv. Manuf. Technol.*, vol. 46, no. 9, pp. 945–956, 2010.

[35] M.-Y. Cheng *et al.*, "Design and fabrication of an artificial skin using PI-copper films," in *Proc. IEEE MEMS*, Jan. 2007, pp. 389–392.
[36] Y.-J. Yang *et al.*, "An integrated flexible temperature and tactile sensing array using PI-copper films," *Sens. Actuators A, Phys.*, vol. 143, pp. 143–153, May 2008.
[37] W.-P. Shih *et al.*, "Flexible temperature sensor array based on a graphite-polydimethylsiloxane composite," *Sensors*, vol. 10, no. 4, pp. 3597–3610, Apr. 2010.
[38] M.-Y. Cheng, C.-M. Tsao, Y.-Z. Lai, and Y.-J. Yang, "The development of a highly twistable tactile sensing array with stretchable helical electrodes," *Sens. Actuators A, Phys.*, vol. 166, no. 2, pp. 226–233, Apr. 2011.
[39] R. Beccherelli *et al.*, "Design of a very large chemical sensor system for mimicking biological olfaction," *Sens. Actuators B, Chem.*, vol. 146, no. 2, pp. 446–452, 2010.
[40] F. Conso, M. Grassi, P. Malcovati, and A. Baschirotto, "A very high dynamic range interface circuit for resistive gas sensor matrix readout," in *Proc. IEEE Int. Symp. Circuits Syst. (ISCAS)*, May 2011, pp. 2209–2212.
[41] L. Wang, J. F. Wu, and H. S. Li, "Design of a CCNN online handwritten digit recognizer for a temperature sensing terminal," *Int. J. Innovative Comput., Inf. Control*, vol. 11, no. 6, pp. 2145–2158, 2015.
[42] J. Wu, L. Wang, and J. Li, "A handwriting input method based on the thermal cue of the fingertip," *Measurement*, vol. 91, pp. 557–564, Sep. 2016.
[43] D. Stratos, G. Maria, F. Eleftherios, and L. George, "Comparison of three resistor network division circuits for the readout of 4×4 pixel SiPM arrays," *Nucl. Instrum. Methods Phys. Res. A, Accel. Spectrom. Detect. Assoc. Equip.*, vol. 702, pp. 121–125, Feb. 2013.
[44] R. S. Saxena, R. K. Bhan, and A. Aggrawal, "A new discrete circuit for readout of resistive sensor arrays," *Sens. Actuators A, Phys.*, vol. 149, no. 1, pp. 93–99, 2009.
[45] R. S. Saxena, A. Panwar, S. K. Semwal, P. S. Rana, S. Gupta, and R. K. Bhan, "PSPICE circuit simulation of microbolometer infrared detectors with noise sources," *Infr. Phys. Technol.*, vol. 55, no. 6, pp. 527–532, 2012.
[46] R. S. Saxena, R. K. Bhan, C. R. Jalwania, and S. K. Lomash, "A novel test structure for process control monitor for un-cooled bolometer area array detector technology," *J. Semicond. Technol. Sci.*, vol. 6, no. 4, pp. 299–312, 2006.
[47] S. Wang, M. Berentsen, and T. Kaiser, "Signal processing algorithms for fire localization using temperature sensor arrays," *Fire Safety J.*, vol. 40, no. 8, pp. 689–697, 2005.
[48] Y. Kato, T. Mukai, T. Hayakawa, and T. Shibata, "Tactile sensor without wire and sensing element in the tactile region based on EIT method," in *Proc. IEEE SENSORS*, Oct. 2007, pp. 792–795.
[49] R. S. Saxena, N. K. Saini, and R. K. Bhan, "Analysis of crosstalk in networked arrays of resistive sensors," *IEEE Sensors J.*, vol. 11, no. 4, pp. 920–924, Apr. 2011.
[50] R. S. Saxena *et al.*, "Characterization of area arrays of microbolometer-based un-cooled IR detectors without using ROIC," *Sens. Actuators A, Phys.*, vol. 141, no. 2, pp. 359–366, 2008.
[51] J. F. Wu, L. Wang, and J. Q. Li, "VF-NSE method measurement error analysis of networked resistive sensor array," *Sens. Actuators A, Phys.*, vol. 211, no. 5, pp. 45–50, 2014.
[52] L. Pan *et al.*, "An ultra-sensitive resistive pressure sensor based on hollow-sphere microstructure induced elasticity in conducting polymer film," *Nature Commun.*, vol. 5, Jan. 2014, Art. no. 3002.
[53] T. Bhattacharjee, A. Jain, S. Vaish, M. D. Killpack, and C. C. Kemp, "Tactile sensing over articulated joints with stretchable sensors," in *Proc. World Haptics Conf. (WHC)*, Daejeon, South Korea, Apr. 2013, pp. 103–108.
[54] A. Jain *et al.*, "Reaching in clutter with whole-arm tactile sensing," *Int. J. Robot. Res.*, vol. 32, no. 4, pp. 458–482, 2013.
[55] S. Dogramadzi, G. Virk, G. Bell, R. S. Rowland, and J. Hancock, "Recording forces exerted on the bowel wall during colonoscopy: *in vitro* evaluation," *Int. J. Med. Robot. Comput. Assist. Surgery*, vol. 1, no. 4, pp. 89–97, 2005.
[56] J. T. Muth *el al.*, "3D Printing: Embedded 3D printing of strain sensors within highly stretchable elastomers," *Adv. Mater.*, vol. 26, no. 36, p. 6202, 2014.
[57] A. Serb, W. Redman-White, C. Papavassiliou, and T. Prodromakis, "Practical determination of individual element resistive states in selectorless RRAM arrays," *IEEE Trans. Circuits Syst. I, Reg. Papers*, vol. 63, no. 6, pp. 827–835, Jun. 2016.
[58] M. A. Zidan, A. M. Eltawil, F. Kurdahi, H. A. H. Fahmy, and K. N. Salama, "Memristor multiport readout: A closed-form solution for sneak paths," *IEEE Trans. Nanotechnol.*, vol. 13, no. 2, pp. 274–282, Mar. 2014.
[59] F. Wang, Y. Song, Z. Zhang, and W. Chen, "Structure analysis and decoupling research of a novel flexible tactile sensor array," *J. Sensors*, vol. 2015, May 2015, Art. no. 476403.

Jian-Feng Wu received the B.S., M.S., and Ph.D. degrees in measurement technology and instrument from the School of Instrument Science and Engineering, Southeast University, Nanjing, China, in 1998, 2003, and 2008, respectively. Since 2014, he has been an Associate Professor with the School of Instrument Science and Engineering, Southeast University. His current research interests include distributed measurement, robots, and wireless sensor networks.